Mechanics Research Communications 131 (2023) 104153

Contents lists available at ScienceDirect

Mechanics Research Communications

journal homepage: www.elsevier.com/locate/mechrescom

An integrated methodology to estimate the effective elastic parameters of amorphous TiO_2 nanostructured films, combining SEM images, finite element simulations and homogenization techniques

Nicola Cefis [a,*], Roberto Fedele [a], Marco G. Beghi [b]

[a] Department of Civil and Environmental Engineering, Politecnico di Milano, Piazza Leonardo da Vinci 32, 20133 Milan, Italy
[b] Department of Energy, Politecnico di Milano, Piazza Leonardo da Vinci 32, 20133 Milan, Italy

ARTICLE INFO

Keywords:
Nano-structured thin film
Amorphous titanium dioxide
SEM images digitalization
Numerical homogenization
Parameter identification

ABSTRACT

In this paper, a novel experimental-numerical methodology is outlined, which aims at estimating the homogenized elastic properties of thin nanostructured coatings, utilized in a variety of industrial contexts. Focus is posed on amorphous titanium dioxide (TiO_2) films, a few micrometer thick, produced through Pulsed Laser Deposition in the form of columnar elements coating a Silicon flat substrate. The proposed inverse strategy rests on digital images acquired by a Scanning Electron Microscope on coated samples, with a nanometer resolution, and consists of the following steps: (i) within a representative volume element, cavities existing in between the nanostructured columns are identified in the raster images by an automatic edge detection procedure; (ii) information concerning the location of the pore borders are vectorized and passed through a Python script to a commercial finite element code; (iii) the homogenized stiffness matrix is reconstructed on the basis of finite element simulations of such a representative volume subjected to elementary loading conditions, each corresponding to a single component of the effective strain tensor. Diverse mechanical models with periodic boundary conditions have been comparatively assessed, fully three dimensional or under plane conditions, assuming for the TiO_2 columns in an amorphous state (as corroborated by Raman spectroscopy) an isotropic behaviour, with a priori known Young's modulus and Poisson's ratio. The homogenized elastic moduli and coefficients of TiO_2 thin films, at varying the deposition process parameter, are estimated by the novel procedure, resulting in an orthotropic, transversely-isotropic behaviour.

1. Introduction

Thin films (i.e. with a micrometer thickness) are being widely utilized for several industrial applications as a non invasive shielding of structural elements: the aim is to improve durability and service life against aggressive chemical–physical agents, which favour wear, corrosion and cracking. It is surprising that a few micrometer layer can affect the long term response of a component. The reason is that several deterioration phenomena initiate from very small defects over the outer surface, followed by a progressive and finally catastrophic development: hence, a delay in the initiation affects the entire process. Moreover, in several scenarios rapid and cheap interventions are expected to restore coatings into their original state, when damaged. More recently, nanostructured coatings, namely films constituted by a modular, nearly periodic structure at a sub-micrometer scale, have attracted the attention of researchers. In the modern spirit of metamaterials [1], nanostructured coatings possess properties which do not exist in nature, and for a variety of engineering applications they exhibit advantages with respect to the monolithic films, e.g. see [2,3].

Once understood the potential advantages of thin films, the development and exploitation of films and coatings have being increasing significantly. The variety of coating materials and of their substrates is expanding, together with the techniques of deposition and the range of thicknesses (from tens of micrometers down to the sub-micrometer range). Some applications, like protections against wear or against corrosion, are more "structural": they require compact and homogeneous films, the effectiveness of which crucially depends on a full and continuous coverage, and on the mechanical integrity. Other applications are more "functional": for several of them, like e.g. the electrochemical, or the catalytical, or the photovoltaic ones, nanostructured films turn out to be more effective, often because they have a larger specific area, see e.g. [4,5].

Among the various techniques apt to deposit thin films, laser ablation, referred to as Pulsed Laser Deposition (PLD), offers a significant

* Corresponding author.
E-mail address: nicola.cefis@polimi.it (N. Cefis).

https://doi.org/10.1016/j.mechrescom.2023.104153
Received 30 March 2023; Received in revised form 29 May 2023; Accepted 15 June 2023
Available online 19 June 2023

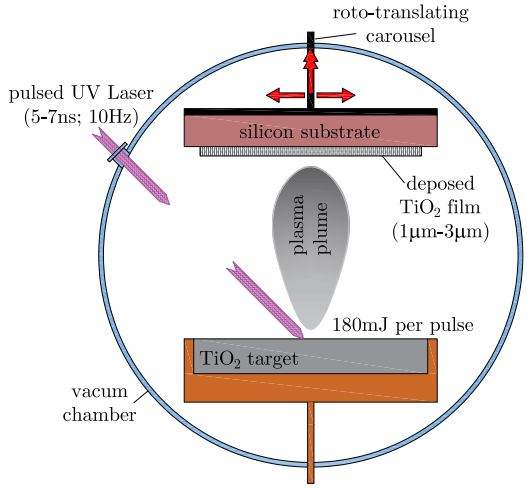

Fig. 1. Working scheme of the Pulsed Laser Deposition (PLD). In the present investigation the deposition chamber, after being evacuated, is kept at a constant pressure of a few Pascals.

flexibility to tune the morphology and the structure, and therefore the functionality of the deposited coatings, see e.g. [6]. By this technique, basically, a target is ablated by a sequence of short (nanoseconds down to femtoseconds) intense laser pulses, and the film is deposited on a substrate, as illustrated in Fig. 1. Indeed, each laser pulse suddenly deposits a significant amount of energy in a shallow surface layer, generating conditions far from equilibrium: as a consequence of this, an ionized plume of plasma is ejected, which expands till reaching the substrate. One of the advantages of this technique is the accurate replication of the stoichiometry of the target (i.e. without altering its chemical composition), possibly corrected by leaving, in the deposition chamber, a residual pressure of a reactive gas. Another advantage is precisely the availability of several process parameters, which can be tuned to control the properties of the deposited coating.

In vacuum the ablation plume expands freely at supersonic speed. The ions and atoms have a significant energy, which allows them, upon arrival onto the substrate, and even without heating the substrate, to reorganize themselves, obtaining compact and dense films. If instead a reactive or non reactive gas is kept in the deposition chamber, at pressures ranging from a fraction of a Pascal to tens of Pascal, the expanding species collide with the gas molecules, losing part of their energy. Depending on the deposition conditions, in vacuum or at very low gas pressures, compact films are obtained which can have either crystalline or amorphous structure. The latter is the outcome of the very fast cooling upon the impact of the expanding plume on the substrate. At higher gas pressures, the energy loss of the expanding ions and atoms is more severe, till clusters can possibly nucleate within the plume itself. These clusters reach the surface with an energy which is not sufficient to fragment them: the film thus grows cluster by cluster, instead of atom by atom, obtaining nanostructured films.

In particular, the collision between the initial supersonic expansion and the residual gas in the chamber generates a shock wave, which delimits the expanding plume. The position of the shock wave depends on the composition of the target, on the parameters of the laser pulse, and on the nature and pressure of the gas. A further tunable parameter is the position of the substrate, which can be kept within the plume, before the shock wave, or beyond it. Alternatively, the substrate can be kept in a fixed position, while controlling the position of the shock wave by modulating the gas pressure in the chamber. When the substrate is within the plume, the obtained coatings are typically compact and homogeneous. When the distance is increased, or equivalently the plume is made smaller by increasing the gas pressure in the chamber, coatings are obtained which have a columnar structure, with a cauliflower external surface. In the resulting nanostructure, columns are first tightly packed, then, at increasing pressures, they can become branched and more loosely connected; pores run between the columns, which exhibit a non-circular cylindrical shape. At higher pressures, foam like films can eventually be obtained, see e.g. [4,5].

When compact, i.e. continuous films are needed, whose integrity is crucial, the mechanical behaviour is of the outmost importance, and is typically investigated. In the case of nanostructured films, functional properties like the specific area are typically more significant than the mechanical behaviour. However, also in these cases, the integrity and the adhesion of the films are relevant, and the assessment of the mechanical properties cannot be neglected.

In compact thin films, the elastic properties are independent from the scale at which they are measured, i.e. they can be regarded as a homogeneous material at any scale, and anisotropy can be dictated by the crystalline structure, if some significant texture is present (let alone the single crystals case). In nanostructured materials the elastic properties depend instead on the scale. At a sufficiently small scale, the properties are those of the single constituents, and therefore can be significantly position dependent. At larger scales, the properties of a nanostructured material approach those of a homogeneous equivalent medium. In particular, in columnar films the average diameter of such columns sets a length scale. At a scale appreciably larger than the average diameter, any volume encompasses both solid columns and intercolumnar spaces, with different properties: they can be either layers of lower stiffness, or cylindrical pores. At these scales the mechanical response approaches that of an effective medium, which can be considered to be statistically homogeneous. This medium can exhibit a significant anisotropy: the properties in the direction of the columns can be appreciably different from those in the transverse plane. The anisotropy due to mesoscopic features, namely to the presence of clusters of columns surrounded by voids, typically prevails over possible crystalline anisotropies of the single columns.

The state of the art approach considers thin films as isotropic materials, see e.g. [7–9]. This assumption permits to simplify considerably, for instance, the interpretation of data provided by Brillouin scattering. However, such an approximation frequently does not correspond to the actual behaviour of nanostructured films. In fact, the elastic response of thin films depends on both the geometric morphology and the crystalline/amorphous properties of the bulk material. Whilst compact films with amorphous or polycrystalline growth, due to the absence of principal orientations, tend to exhibit an isotropic behaviour, for the compact films with epitaxial growth (due to principal orientations of the material) and for the nanostructured films with columnar growth (due to the morphology) an anisotropic behaviour is expected. We believe that, to further improve the use and technology of these thin coatings, an accurate mechanical modelling is crucial.

For a qualitative or morphological assessment of thin films, SEM images with nanometer resolution are utilized very often, as a fundamental tool, whilst seldom they are used after segmentation to evaluate quantitatively the pore distribution: even more rarely, such images are processed to generate a finite element model suitable to run thermo-mechanical simulations, see e.g. [10] with reference to compact coatings. However, to the authors' knowledge, the actual nanostructures of the coating are not modelled in detail, and an idealized geometry of such elements is preferred for the simulations, as in [11].

Titanium dioxide (TiO_2) has attracted the interest of researchers due to its peculiar physico-chemical properties: currently, it is used in optics, to realize filters and anti-reflection coatings, for photocatalysis and photovoltaic (solar cells), in medicine, as biocompatible films for biomaterials, and in electronics, for Metal-Oxide-Semiconductor capacitors. In this study a novel experimental-numerical methodology is outlined to estimate the homogenized elastic properties of such thin films, resting on SEM images of the coating with nanometer resolution. The contribution is organized as follows. Section 2 is devoted to the

Table 1
List of coated samples (ID: identification number; p: deposition chamber pressure; t: actual thickness).

ID	TI1_7	TI3_5	TI3_7	TI3_10
p	7 Pa	5 Pa	7 Pa	10 Pa
t	1.13 μm	3.81 μm	3.49 μm	4.04 μm

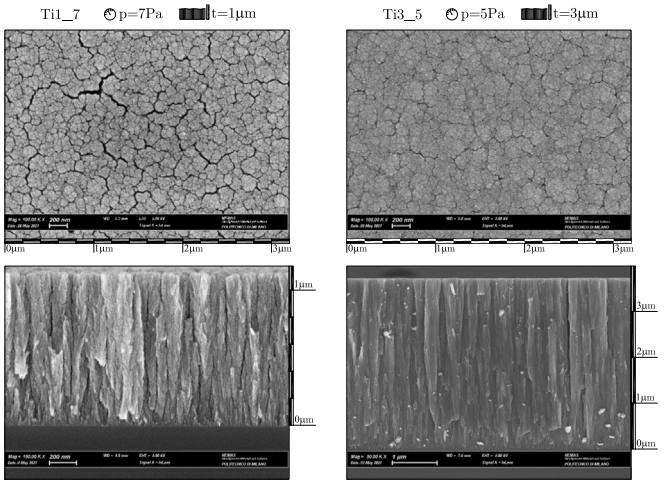

Fig. 2. Frontal views and cross sections by SEM of TI1_7 and TI3_5 samples. Chamber pressure p and final thickness t of the film are reported at the top of the frontal view.

sample preparation and characterization. In Section 3, an automatic edge detection procedure, based on grayscale intensities of digital images, is presented, to identify the pores in the representative volume element. In Section 4, such information is passed to a finite element code, and two basic models of the nanostructured film are developed, exploiting periodic boundary conditions. Assuming from the literature the bulk mechanical properties of amorphous titanium dioxide, homogenized moduli and coefficients of the thin film are computed though the repeated simulation of elementary loading conditions, in order to assess the possible geometry-induced anisotropy at the macroscale.

2. Sample preparation and characterization

Previous work [4] on the deposition by PLD of TiO_2 films have identified a relatively narrow interval of gas pressures, from 5 to 10 [Pa], in which the structure of the deposited coatings changes from an already columnar structure, but with tightly packed columns, to more open structures, which include porosity in the form of "channels" among columns. In all these cases the columnar structure is expected to generate in the film as a whole a significant anisotropy.

Following these findings, at the *Micro and Nanostructured Materials Lab* of Politecnico di Milano an experimental campaign has been carried out, depositing TiO_2 films by PLD at the pressures of 5, 7 and 10 [Pa], and characterizing their morphology on the basis of SEM images. Films with 3 [μm] nominal thickness were grown at the three pressures, together with a film of 1 [μm], at the intermediate pressure of 7 [Pa], to be regarded as a reference. Films were deposited on a Si(001) substrate, by a pulsed UV laser (wavelength 266 [nm]), with pulse duration of 5–7 [ns], a fluence, for each pulse, of 180 [mJ], and a pulsation frequency $\nu = 10$ [Hz].

The morphology of the nanostructured films was characterized by means of a Zeiss field-emission Scanning Electron Microscope (fe-SEM 40), providing grayscale images with 1024 × 768 [pixel], 8-bit digitization. In what follows, to avoid any ambiguity the top views of the coating texture as resulting from SEM images will be referred to as *frontal views*, the lateral views comprehensive of the thickness as *cross sections*, whilst the frontier of the voids included in these images will be

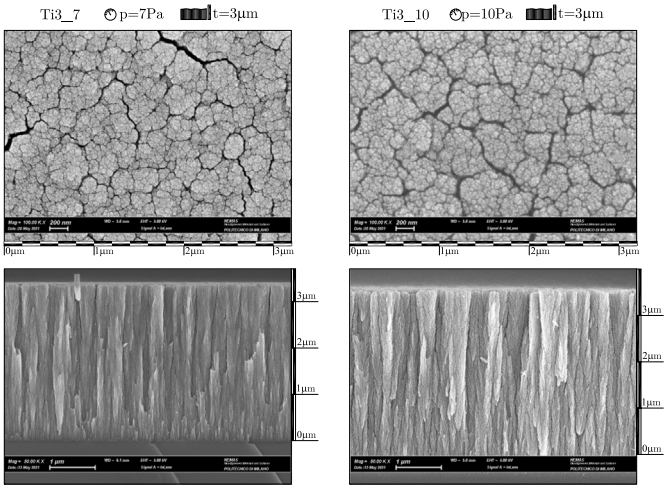

Fig. 3. Frontal views and cross sections by SEM of TI3_7 and TI3_10 samples. Chamber pressure p and final thickness t of the film are also reported at the top of the frontal view.

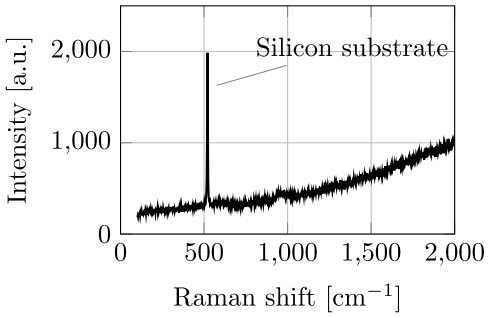

Fig. 4. Raman spectrum for sample Ti3_5.

denominated *void border*. Frontal views and cross sections, for all the samples, are presented in Figs. 2 and 3, with a resolution ranging from 1.6 to 5 [nm]/pixel.

The frontal views mostly include light grey portions, corresponding to the solid regions, and dark grey portions, corresponding to the cavities consisting of pores or interfaces. By visual inspection, a sharp contrast can be noticed between the above two regions. The cross sections show a columnar morphology with parallel channels that can be considered, in a first approximation, perpendicular to the Silicon substrate and passing throughout the entire thickness. The coatings, a few micrometre thick, consist of columns having a diameter of about 100 [nm], with a roughly polygonal cross section, placed side by side to cover the substrate almost uniformly, except for the presence of almost cylindrical pores which are visible by SEM in the outer surface of the coating. From SEM images, the appearance of the outer surface is rather jagged, and each columnar structure (as identifiable from the cross sections) seems, when seen from above, actually constituted by tens of unequal buds, each one approximately 10–30 nm thick. In agreement with previous observations [4], films deposited at increasing pressures are characterized by a marked increase of the porosity. At 5 [Pa] porosity is almost undiscernible by visual inspection, while at 10 [Pa] the columns exhibit an accentuated tendency to aggregate into compact islands, surrounded by pores appearing as cracks with multiple branches.

To assess the type of structure (crystalline or amorphous), the coated samples were also characterized by Raman spectroscopy, with an Argon laser at the wavelength of 514 [nm]. The spectrum presented in Fig. 4 is representative of those obtained for all the samples. A unique sharp peak is present, which is due to the crystalline Silicon of the

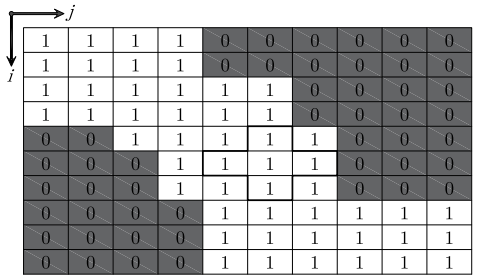

(a) Binarized image, including pores, with value 1 (white coloured), and matrix, with value 0 (dark gray). The moving mask, conventionally defining the neighborhood of each pixel, is also shown, with a marked border.

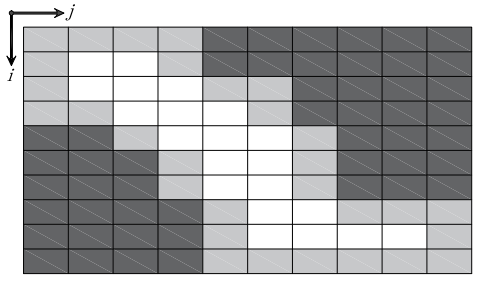

(b) Pixels at the pore border, marked by light gray colour.

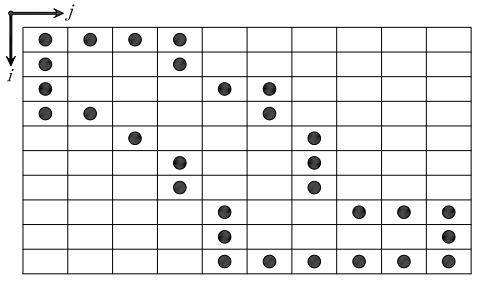

(c) Identified pore border locations.

Fig. 5. Computation of pore border coordinates from a generic pixel pattern.

substrate (peak at about 520 [cm^{-1}]), and which can be exploited to calibrate the spectra. This circumstance allows one to conclude that, differently from previous depositions [4], the titanium dioxide of the coating is in an amorphous state. The bulk material is thus, locally, isotropic: however, due to the columnar structure, the film as a whole is expected to behave anisotropically.

3. Pore border identification and vectorization

To develop a suitable computational model of the film, firstly we need an accurate description of the actual geometry inside a representative volume element. Starting from the original raster images, provided by SEM in a .TIFF format and concerning the frontal view of the film, the border of the pores is identified by an automatic edge detection procedure, which exploits exclusively grayscale intensities and has been implemented by the authors in a Matlab® environment.

The procedure consists of the following steps, illustrated in Fig. 5. (i) The 8-bit SEM images are binarized, by selecting a suitable segmentation threshold on the basis of the relevant histogram. It is worth emphasizing that the possible presence of a physical discontinuity usually results in intermediate grayscale values at the specific location of a digital image, due to the physical size of the pixel at the detector. (ii) Within the binarized image, pixels located at the pore borders are identified. The following criterion is utilized: pixel at the location

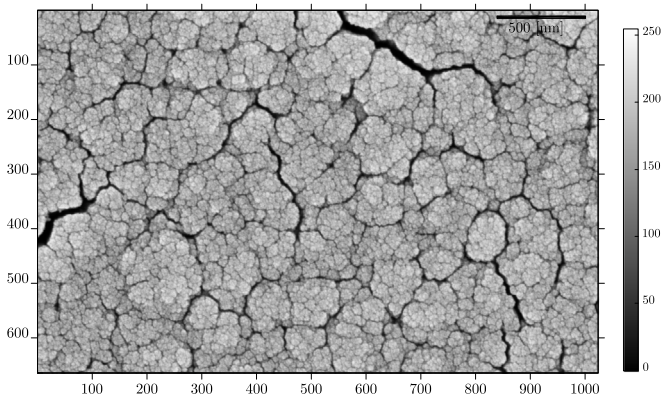

Fig. 6. SEM image, in 8-bit grayscale intensities, of TI3_7 surface. Pixel size 3.125 [nm].

(i, j) belongs to the interior of a pore (and not to its border) if its four surrounding pixels, located along the axes of the 3 × 3 sub-block centered in it, belong to the pore. In Fig. 5(a) the considered cross-shaped mask is indicated. In practice, this criterion involves the grayscale intensities of the surrounding pixels at the locations $(i \pm 1, j)$ and $(i, j \pm 1)$: consistently, a pixel in a pore is assigned to the pore border, if at least one of its surrounding pixels belongs to the matrix. Moreover, if at least one of the surrounding pixels lies out of range with respect to the image frame, pixel at the location (i, j) is assigned to the border. (iii) The integer coordinates of the border pixels within the discrete image are then converted into real coordinates in the physical space. (iv) From the coordinates of the border pixels, differently from [12], a vector file in .DXF format is generated. Such a .DXF file contains in an ASCII format all the information (coordinates of points, connectivity, graphic styles) necessary for the generation of geometric sketches and the visualization of a vector drawing in a CAD environment. (v) With the aid of a Python script, see e.g. [13], the .DXF file is imported into the CAE pre-processor of the Abaqus® environment [14]. (vi) Combining the information provided by the frontal views with the cross sections (Figs. 2 and 3), the frontal geometry of the columnar nanostructure (as detected over the free surface) was extruded to build a three dimensional model of the film.

The pore border detection procedure was firstly validated on the basis of synthetic images, containing circular inclusions of different size assigned a priori, possibly perturbed by noise with increasing intensity. For a comparative assessment, recourse was made also to the built-in function *contour* available in the Matlab image processing toolbox, apt to extract contours from a binary image. However, for the selected pictures the two procedures provided coincident results.

Thereafter, experimental SEM images were processed. Fig. 6 shows the frontal view of the coated sample labelled as TI3_7 in Table 1, with thickness t = 3.49 μm and chamber pressure p = 7 [Pa]. The Field-Of-View of the original image, cropped to 1024 × 663 [pixel] due to the SEM legend, corresponds in the physical space to an area with dimensions 3.200 × 2.072 μm. Fig. 7 shows the pore borders identified by the present procedure, with the matrix white coloured.

4. Mechanical models and homogenized properties

The generation of a suitable mechanical model for the thin film is carried out by extracting a representative part of the .DXF file, importing it into the CAE pre-processor of the commercial finite element code Abaqus®, and possibly extruding it along the out-of-plane direction, up to a suitable length. The mechanical modelling of the thin film can be developed in two basic ways, useful for a comparative assessment: (i) a 2D model, under plane strain or plane stress conditions, with periodic boundary conditions involving the nodal displacements in this plane

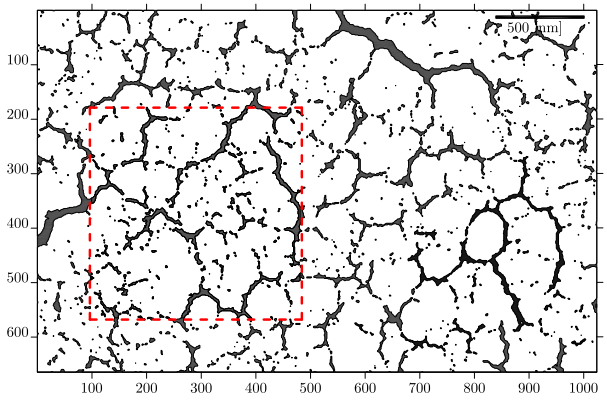

Fig. 7. Pore borders identified by the automatic edge detection procedure on the basis of the SEM frontal view in Fig. 6. The matrix is white coloured, and the representative square region selected for the mechanical model (with 1200 [nm] size) is marked by red. (For interpretation of the references to colour in this figure legend, the reader is referred to the web version of this article.)

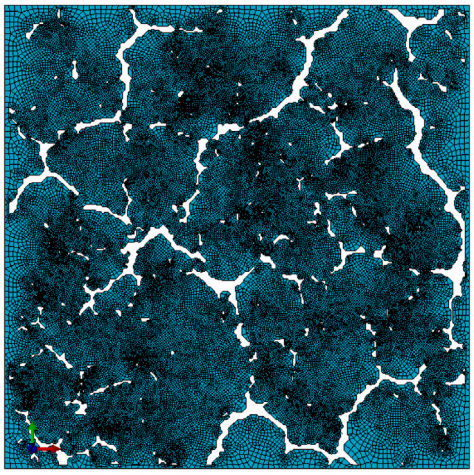

Fig. 8. 2D finite element discretization of a representative region for the coated sample TI3_7. In plane size of the square region amounts to 1.2 [μm].

(see e.g. [15]); (ii) a three dimensional model, where the extruded side (out-of-plane with respect to the frontal view) can be assumed small with respect to the actual coating thickness, exploiting the geometric and material periodicity also through the coating thickness (and extrusion direction). As for the point (i), the plane stress approximation can be of interest in order to calibrate material properties on the basis of full-field kinematic measurements over the sample free surface, provided e.g. by 2D Digital Image Correlation (as in [16,17]) combined with an *in situ* microtesting apparatus, ad-hoc designed for the microscope. As for the model (ii), it is worth emphasizing that the periodicity conditions involve all the nodal boundary displacements.

A Python script developed by the authors has permitted to specify the periodicity boundary conditions, in the form of a system of linear equations constraining displacements at the corresponding nodes over opposite faces of the representative volume element, for the three dimensional model, or along opposite sides of a square element for the plane models. Thereafter, the degrees of freedom at the boundary nodes left independent are utilized to prescribe a unit component of the effective strain tensor to the representative volume element: the reaction forces corresponding to such boundary displacements generate the columns of the homogenized stiffness matrix. By this strategy the integral average of the microscopic stress fields is no more needed, thus reducing significantly the computing effort of the homogenization procedure.

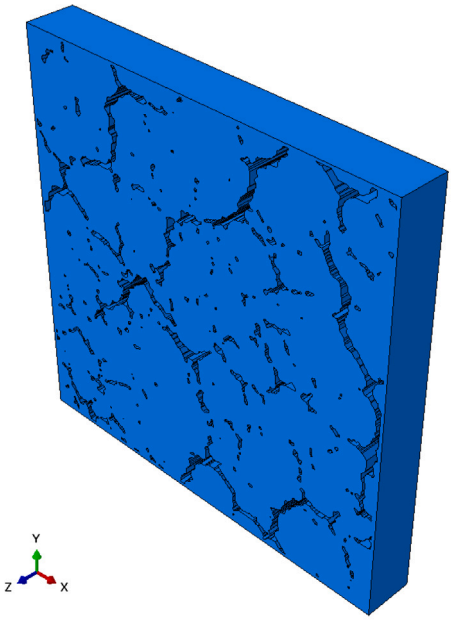

(a) Solid volume of the coating matrix generated by extrusion along the z axis of the segmented image in Fig. 7. In plane size 1.2 [μm], out-of-plane thickness 150 [nm], corresponding to about 1/23 of the nominal coating thickness.

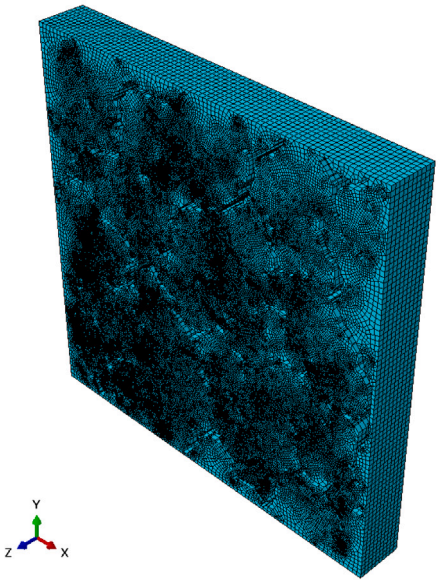

(b) Finite element discretization by hexaedral elements of the above volume.

Fig. 9. Three dimensional finite element model of the representative volume element (with periodic boundary conditions) for the coated sample TI3_7.

To illustrate the modelling stage, let us make reference to the coated sample TI3_7, whose frontal view by SEM and identified pore borders are visualized in Figs. 6 and 7. The plain model, shown in Fig. 8, includes 56,542 quadrilateral elements (named CPE4 and CPS4 in the Abaqus element library, in turn for plane strain and plane stress): for each loading condition, the finite element analysis has required about 20 s on an Intel core I9-10980XE processor, with a 3.0 GHz clock, 128 GB RAM. The relevant three dimensional model built by extrusion, shown in Fig. 9, consists of 571, 580 hexaedral elements (named C3D8 in the Abaqus library) and 651, 706 nodes. The out-of-plane length of the solid model, assumed equal to t = 0.15 μm, represents a small part of the actual coating thickness. For this model each forward analysis,

Table 2
Effective moduli and Poisson's coefficients for the orthotropic response identified through the three-dimensional representative volume element in Fig. 9. Symbol ϕ indicates the porosity, whilst symbol $\widetilde{E}_{zz}$ denotes the Young's modulus along the direction z predicted by the mixture rule.

ID	TI1_7	TI3_5	TI3_7	TI3_10
E_{xx} [GPa]	25.33	69.46	35.93	19.04
ν_{xy}	0.05	0.23	0.13	0.13
ν_{xz}	0.05	0.14	0.07	0.04
E_{yy} [GPa]	29.43	54.89	45.29	24.96
ν_{yx}	0.06	0.18	0.17	0.17
ν_{yz}	0.06	0.11	0.09	0.05
E_{zz} [GPa]	128.19	133.99	138.22	127.10
ν_{zx}	0.27	0.27	0.27	0.27
ν_{zy}	0.27	0.27	0.27	0.27
G_{xy} [GPa]	8.46	20.23	18.37	4.91
G_{xz} [GPa]	22.15	35.61	24.28	16.17
G_{yz} [GPa]	19.40	32.01	29.00	18.46
ϕ [%]	13.98	11.52	9.01	15.95
$\widetilde{E}_{zz}$ [GPa]	129.89	133.60	137.40	126.92

corresponding to a singular loading condition, on the same server has required about 3 h. Besides the increased number of degrees of freedoms, such a large computing time is also due to a number of equations constraining the displacements of the boundary nodes significantly larger than in the bidimensional case, needed to implement the periodicity conditions along the three directions.

The amorphous structure of the film makes it possible to consider an isotropic linearly elastic behaviour for the TiO_2 columns, assuming a priori values of Young's modulus and the Poisson's ratio as in [18], namely $E^{TiO_2} = 151$ [GPa] and $\nu^{TiO_2} = 0.27$. On the basis of such an assumption, the homogenized elastic moduli and coefficients, obeying to a fully orthotropic behaviour, have been identified by the proposed inverse methodology resting on the three dimensional model, and are reported in Table 2. As well known, there are nine independent elastic parameters, or, equivalently, twelve parameters constrained by the major symmetry of the compliance matrix. It is worth emphasizing that, for each coated sample, such analyses have been carried out starting from a specific representative volume. At the light of this fact, we can interpret, for instance, the circumstance that the estimated porosity ϕ in Table 2 is not monotonically increasing, as expected, with the pressure in the deposition chamber. To assess the estimation uncertainty related to the above strategy, the procedure should be repeated several times, by processing a different representative area within the same picture, maintaining constant its size: thereafter, the resulting population of data could be characterized statistically by suitable sampling operators. In any case, on the basis of such preliminary results, the difference between the Young moduli within the plane $\{x, y\}$ amounts to about 20 [%], and for the above reasons it can be considered to be negligible, especially if compared to the out-of-plane stiffness, which turns out to be several times higher. Hence, the behaviour of the nanostructured film in the plane $\{x, y\}$ can be considered to be isotropic within a reasonable approximation, giving rise to an orthotropic, transversally isotropic behaviour at the macroscale. The Young's modulus along the out-of-plane direction results in agreement with the prediction provided by the mixture rule $\widetilde{E}_{zz}$, based on the current porosity ϕ and on the bulk modulus of the amorphous TiO_2, $E^{TiO_2} = 151$ [GPa]. At increasing pressures during the deposition process, the resulting nanostructured films exhibit an increased porosity, which implies progressively lower homogenized moduli and Poisson's ratios. When passing from film labelled as TI3_5 to TI3_10, the ratio E_{xx}/E_{yy} decreases approximately by 40%: this circumstance suggests that, at increasing the film porosity, the degree of anisotropy within the plane $\{x, y\}$ becomes weaker and weaker, whilst the fluctuations of the out-of-plane moduli turn out to be negligible. The above results can be compared to those obtained under plane strain and plane stress approximations, based on the 2D model in Fig. 8, where the periodic boundary conditions involve the in-plane nodal displacements. The in-plane homogenized moduli and coefficients for the coated sample TI3_7 are reported in Table 3.

Table 3
Coated sample TI3_7: homogenized moduli and coefficients for the plane orthotropic response identified through the 2D representative element, under plane strain and plane stress assumptions.

TI3_7	Plane strain	Plane stress
E_{xx} [GPa]	36.92	34.22
ν_{xy}	0.16	0.13
E_{yy} [GPa]	46.67	43.25
ν_{yx}	0.20	0.17
G_{xy} [GPa]	18.54	17.58

As expected, in Table 3 the elastic moduli under plain strain conditions turn out to be slightly higher than their plane stress counterparts. Moreover, the in-plane moduli and coefficients estimated through the 2D model are close to the corresponding stiffness elements provided by the fully three dimensional model, with discrepancies lower than 10%.

5. Closing remarks and future prospects

In this study a novel procedure is outlined, suitable to identify the homogenized elastic moduli and Poisson's ratios of nanostructured thin films with a columnar morphology. The proposed methodology, obeying to a micro-macro strategy, is based on finite element models of a representative volume element, which exploit the film texture as resulting through SEM images by means of an automatic edge detection procedure. Reference is made to thin coatings over a Silicon substrate, constituted of TiO_2 columns grown by PLD, at varying the deposition process parameters. For the considered films the TiO_2 columns result in an amorphus state, as confirmed by Raman spectroscopy, and their isotropic bulk properties have been assumed from literature data. Starting from a fully orthotropic behaviour, the estimated moduli indicate within a reasonable approximation a transverse isotropy of the film, especially at increasing pressures as crucial deposition process parameter.

The present results, although very promising, have to be considered as still preliminary, and need further validation. In particular, the proposed inverse procedure is based on a sufficiently wide representative area over the frontal view of the nanostructured coating, selected by the user within the available SEM images. The reference length for this choice is represented by the average diameter of the tubular TiO_2 structures, which amounts to about 100 nm, as it can be estimated in the coating cross sections: hence, the side of the representative region selected in the frontal view, equal to about 1.2 micrometers, turns out to be one order of magnitude larger. As a further improvement, one could try to assess the dependence of the results on the size of the representative area, and, at equal size, on its location within the monitored region. In this way, the estimated parameters could be endowed by a measure of uncertainty (e.g. through a covariance matrix), exploiting also their mutual correlation.

It is worth noting that, with respect to above mentioned diameter of the TiO_2 columns, the acoustic excitations probed by Brillouin scattering, with wavelengths of few hundred nanometres, can still be treated as those of an effective homogeneous medium [19]. For this reason, the experimental characterization of these films by Brillouin spectroscopy (see e.g. [6,20]) is on course, with the final aim to provide an alternative assessment of the effective mechanical properties in the presence of anisotropy. Such information can be integrated also by nanoindentation experiments, as suggested in [21], although the response to nanoindentation of anisotropic thin films is still under investigation.

Besides that, the elastic parameters of the nanostructured film should enter a mechanical model of the coated structural element, for instance governing a zero-thickness interface, similarly to what already developed for other typologies of joined assemblies [22,23].

Declaration of competing interest

The authors declare that they have no known competing financial interests or personal relationships that could have appeared to influence the work reported in this paper.

Data availability

Data will be made available on request

References

[1] E. Barchiesi, M. Spagnuolo, L. Placidi, Mechanical metamaterials: a state of the art, Math. Mech. Solids 24 (1) (2019) 212–234, http://dx.doi.org/10.1177/1081286517735695.

[2] B. Paladino, M. Vanazzi, D. Iadicicco, A. Perinot, M. Caironi, L. Ceseracciu, P. Reccagni, S. Bassini, M. Utili, F. Di Fonzo, Design of a PLD–grown Y2O3 protective barrier for fusion relevant applications, Nucl. Fusion 60 (2020) 106018, http://dx.doi.org/10.1088/1741-4326/abab51.

[3] M. Utili, S. Bassini, S. Cataldo, F.Di. Fonzo, M. Kordac, T. Hernandez, K. Kunzova, J. Lorenz, D. Martelli, B. Paladino, A. Morono, M. Tarantino, C. Schroer, G.A. Spagnuolo, L. Vala, M. Vanazzi, A. Venturini, Development of anti-permeation and corrosion barrier coatings for the WCLL breeding blanket of the European DEMO, Fusion Eng. Des. 170 (2021) 112453, http://dx.doi.org/10.1016/j.fusengdes.2021.112453.

[4] L. Passoni, F. Ghods, P. Docampo, A. Abrusci, J. Martí-Rujas, M. Ghidelli, G. Divitini, C. Ducati, S. Binda, A.Li. Bassi, C.S. Casari, H.J. Snaith, A. Petrozza, F. Di Fonzo, Hyperbranched quasi 1D nanostructures for solid-state dye-sensitized solar cells, ACS Nano 7 (11) (2013) 10023–10031, http://dx.doi.org/10.1021/nn403979h.

[5] A. Mezzetti, M. Balandeh, J. Luo, S. Bellani, A. Tacca, G. Divitini, C. Cheng, C. Ducati, L. Meda, H. Fan, F.Di. Fonzo, Hyperbranched TiO_2–CdS nanoheterostructures for highly efficient photoelectrochemical photoanodes, Nanotechnology 29 (2018) 335404, http://dx.doi.org/10.1088/1361-6528/aac852.

[6] E. Besozzi, D. Dellasega, A. Pezzoli, C. Conti, M. Passoni, M.G. Beghi, Amorphous, ultra-nano- and nano-crystalline tungsten-based coatings grown by pulsed laser deposition: mechanical characterization by surface brillouin spectroscopy, Mater. Des. 106 (2016) 14–21, http://dx.doi.org/10.1016/j.matdes.2016.04.096.

[7] L. Borgese, E. Bontempi, M. Gelfi, L.E. Depero, P. Goudeau, G. Geandier, D. Thiaudière, Microstructure and elastic properties of atomic layer deposited TiO2 anatase thin films, Acta Mater. 59 (7) (2011) 2891–2900, http://dx.doi.org/10.1016/j.actamat.2011.01.032.

[8] B.R. Braeckman, P. Djemia, F. Tétard, L. Belliard, D. Depla, Impurity-controlled film growth and elastic properties of CoCrCuFeNi thin films, Surf. Coat. Technol. 315 (2017) 475–483, http://dx.doi.org/10.1016/j.surfcoat.2017.03.014.

[9] A. López-Puerto, F. Avilés, F. Gamboa, A.I. Oliva, A vibrational approach to determine the elastic modulus of individual thin films in multilayers, Thin Solid Films 565 (2014) 228–236, http://dx.doi.org/10.1016/j.tsf.2014.06.024.

[10] A. Abdelgawad, K. Al-Athel, Effect of tgo thickness, pores, and creep on the developed residual stresses in thermal barrier coatings under cyclic loading using SEM image-based finite element model, Ceram. Int. 14 (2021) 20064–20076, http://dx.doi.org/10.1016/j.ceramint.2021.03.336.

[11] V. Fauvel, Y. Gaillard, R. Guillemet, P. Garabédian, F. Richard, Numerical and experimental crossed analysis of coated nanostructures through nanoindentation, Int. J. Mech. Sci. 245 (2023) 108091, http://dx.doi.org/10.1016/j.ijmecsci.2022.108091.

[12] A. Rabbani, S. Salehi, Dynamic modeling of the formation damage and mud cake deposition using filtration theories coupled with SEM image processing, J. Nat. Gas Eng. 42 (2017) 157–168, http://dx.doi.org/10.1016/j.jngse.2017.02.047.

[13] G.M. Puri, Python Scripts for Abaqus. Learn by Example, ISBN 978-0-615-52050-6. http://www.abaquspython.com.

[14] Dassault Systèmes, Abaqus/Standard Users' Manual, Simulia Corporation, San Diego, US, 2021.

[15] R. Fedele, G. Maier, M. Whelan, Calibration of local constitutive models through measurements at the macroscale in heterogeneous media, Comp. Meth. Appl. Mech. Engn. 195 (37–40) (2006) 4971–4990, http://dx.doi.org/10.1016/j.cma.2005.07.026.

[16] R. Fedele, Simultaneous assessment of mechanical properties and boundary conditions based on digital image correlation, Exp. Mech. 55 (1) (2015) 139–153, http://dx.doi.org/10.1007/s11340-014-9931-x.

[17] E. Barchiesi, F. dell'Isola, F. Hild, On the validation of homogenized modeling for bi-pantographic metamaterials via digital image correlation, Int. J. Solids Struct. 208–209 (2021) 49–62, http://dx.doi.org/10.1016/j.ijsolstr.2020.09.036.

[18] L. Borgese, M. Gelfi, P. Bontempi, G. Geandier, D. Thiaudière, L.E. Depero, Young modulus and Poisson ratio measurements of TiO_2 thin films deposited with atomic layer deposition, Surf. Coat. Technol. 206 (8–9) (2012) 2459–2463, http://dx.doi.org/10.1016/j.surfcoat.2011.10.050.

[19] M.G. Cottam, A.A. Maradudin, Surface linear response functions, in: V.M. Agranovich, R. Loudon (Eds.), Surface Excitations, Elsevier, London, 1984.

[20] A.G. Every, L.M. Kotane, J.D. Comins, Characteristic wave speeds in the surface brillouin scattering measurement of elastic constants of crystals, Phys. Rev. B 81 (2010) 224303, http://dx.doi.org/10.1103/PhysRevB.81.224303.

[21] S. Zak, C.O.W. Trost, P. Kreiml, M.J. Cordill, Accurate measurement of thin film mechanical properties using nanoindentation, J. Mater. Res. 37 (2022) 1373–1389, http://dx.doi.org/10.1557/s43578-022-00541-1.

[22] R. Fedele, M. Scaioni, L. Barazzetti, G. Rosati, L. Biolzi, Delamination tests on CFRP-reinforced masonry pillars: optical monitoring and mechanical modelling, Cem. Concr. Compos. 45 (2014) 243–254, http://dx.doi.org/10.1016/j.cemconcomp.2013.10.006.

[23] R. Fedele, L. Galantucci, A. Ciani, V. Casalegno, A. Ventrella, M. Ferraris, Characterization of innovative CFC/Cu joints by full-field measurements and finite elements, Mater. Sci. Eng. A 595C (2014) 306–317, http://dx.doi.org/10.1016/j.msea.2013.12.015.